Hydrophobicity in clearwing Lepidoptera: impact of scale micro and nanostructure, and trade-off with optical transparency

Doris Gomez[1*], Jonathan Pairraire[2], Charline Pinna[3], Monica Arias[1], Céline Houssin[3], Jérôme Barbut[3], Serge Berthier[2], Christine Andraud[4], Thierry Ondarçuhu[5], Marianne Elias[3]

[1] CEFE, CNRS, Univ Montpellier, EPHE, IRD, Montpellier, France, 34090

[2] INSP, Sorbonne University, CNRS, Paris, France, 75005

[3] Institut de Systématique, Evolution, Biodiversité (ISYEB), CNRS, Muséum national d'Histoire naturelle, Sorbonne Université, EPHE, Université des Antilles, France, 75005

[4] CRC, MNHN, Paris, France, 75005

[5] IMFT, Univ. Toulouse, CNRS, Toulouse, France, 31400

Corresponding author: Doris Gomez

Email: doris.gomez@cefe.cnrs.fr

Abstract

While scales ensure hydrophobicity in opaque Lepidoptera, their reduction in clearwing species question hydrophobicity and its dependency on wing microstructures (scale presence, morphology, insertion, coloration) and nanostructures (scale ridge features). By measuring static contact angle (CA) of water droplets at different stages of evaporation in opaque and transparent patches of 23 clearwing species with varied microstructure, we establish for the first time that transparency is costly for hydrophobicity, a cost depending on microstructure: transparent patches lose more hydrophobicity with water evaporation than opaque patches, a loss attenuated for higher scale densities, coloured scales (for erect scales), and when combining two types of scales (piliform and lamellar). Nude membranes show lowest hydrophobicity. Models best predicting CA include microstructures for all scales, and nanostructures only for flat scales. We reveal for the first time that wing hydrophobicity negatively relates to optical transparency. Finally, tropical species have more hydrophobic transparent patches but similarly hydrophobic opaque patches compared to temperate species. All findings are consistent with the physics of hydrophobicity, especially on multiscale roughness, and underline that wings are evolutionary compromises.

Keywords: Lepidoptera; transparency; trade-off; multiscale roughness; hydrophobicity

INTRODUCTION

Hydrophobicity is essential for terrestrial organisms. As predicted by physics (1) and illustrated in plants (2), a key parameter for hydrophobicity is surface texture or roughness. A water droplet sitting on a textured hydrophobic surface can exhibit two different wetting states. First, in the Cassie-Baxter state (Figure 1, series a), the water droplet sits on top of the texture, with trapped air underneath and cavities filled with air (composite state: under the drop, water can be in contact with solid or air), and hydrophobicity is at a maximum. If this state is thermodynamically unstable, the water droplet may undergo the so-called Cassie-Baxter to Wenzel transition, in which water penetrates the air-filled cavities by capillarity. In the Wenzel wetting state (Figure 1 series b), the water droplet fully fills all the cavities of the textured surface and adheres to the surface (non-composite state: under the drop, water is in contact with solid only and no longer with air), decreasing the surface energy; hydrophobicity is then lost (3). Compared to the Wenzel state, the Cassie-Baxter state is of high biological interest as it offers an incomplete water-surface contact and a weak water adhesion. Maintaining a stable Cassie-Baxter state is crucial to maintain high hydrophobicity under harsh environmental conditions, rainfall for instance. Roughness at nanoscale – the parameter most studied to date in animals and plants - increases hydrophobicity, as shown in cicadids and dragonflies (4–6). Yet, multiscale roughness –at nano and micro scale – is even more efficient: it increases hydrophobicity and its thermodynamic stability (in modelling studies 7, 8, illustrated in the Lotus (so-called 'Lotus effect') and other plants in 9) and reduces water adhesion (7). Increasing thermodynamic stability allows maintaining hydrophobicity with water droplets of various sizes (dew, fog, rain) and increases anti-fogging properties, i. e. the resistance to tiny water droplets condensing on the surface. While the role of nanostructures in hydrophobicity has been extensively documented (e.g. 10, 11), the role of microstructures shape in determining hydrophobic properties has been limited to simple geometries (cones in 12, cylinders in 13, 14) and remains poorly investigated from an empirical perspective. The only existing empirical studies with such an approach either focus on one type of micro-architecture (6, 15) thereby excluding microstructural influence, or they describe variation in hydrophobicity between various micro-architectures but without invoking explanations (16).

Lepidoptera (from the ancient Greek λεπίς: scale and πτερόν: wing) – butterflies and moths – offer an outstanding group to investigate this question. They are characterized by wings entirely covered with flat and coloured lamellar scales (17). Through their pigmentation and structure, scales are involved in multiple functions such as antipredator defences (e. g. camouflage, deflection, mimicry in 18, 19), communication (20), thermoregulation (17, 21–23), or flight enhancement (24, 25). They also confer superhydrophobic properties to the wing, resulting in water repellency and self-cleaning (26, 27). Superhydrophobicity *sensu lato* is defined by water droplets making high contact angles (>150°) with a surface. Self-cleaning – superhydrophobicity *stricto sensu* (definition not taken here) –

adds to this condition a weak water adhesion, estimated by a minimal tilt from the horizontal plane needed for water droplets to roll-off (roll-off angle of a few degrees) or a minimal hysteresis (difference between advancing and receding contact angles). Superhydrophobicity is thus a *sine qua non* condition for water repellency and self-cleaning. Opaque butterflies and moths typically have self-cleaning wings, as attested by small roll-off angles (15, 28). Scarce relevant studies suggest that wing hydrophobicity may depend on wing microstructure (presence and type of scale in 26, scale type and insertion angle in 29), and on wing macrostructure: species with longer wings (4), or larger ratio of wing area to body mass (26) show higher hydrophobicity and wing shape was invoked to explain natural variations in hydrophobicity (4).

While the vast majority of Lepidoptera species has opaque wings, some species from various lineages show transparent or translucent wings (30), which reduces their detectability from visually-hunting predators (31–33). Transparency shows a broad microstructural diversity (i. e. scale diversity, see examples in Figure 2), the membrane being nude or covered with scales varying in type (piliform, i. e., hair-like, and/or lamellar), insertion on the membrane (flat or erect), and colouration (coloured or transparent) (30). All combinations of scale type, insertion, and colouration (i. e., structural strategies 30) can be found in nature (Figure 2), and they differ in their efficiency at transmitting light : the nude membrane are most efficient while flat coloured scales (lamellar alone or in combination with piliform) are least efficient (30). Microstructures are complemented by nanostructures: longitudinal ridges on scales, and nanostructures on the wing membrane, of various shape and density. Membrane nanostructures reduce reflection levels and increase light transmission (34–37).

Because transparency often entails profound modifications of scale dimensions and density (30), we can suppose that transparency may be potentially costly for hydrophobicity, for both water repellency and self-cleaning. These functions are vital for butterflies and moths: water repellency is crucial for flight and for preventing wings from sticking together, especially in tropical rainforest species with daily rain and high humidity. Likewise, self-cleaning helps removing dust contamination that impairs flight (26). Among the lepidopteran species investigated so far for hydrophobicity (15, 26, 27, 29, 38), only three clearwing butterfly species have been included: *Parantica sita* (with lamellar titled scales) and *Parnassius glacialis* (with flat lamellar scales), with high or moderate hydrophobicity respectively (15, 29), and *Greta oto* (with piliform scales) with one of the lowest hydrophobicity values found in butterflies (27). Scarce data suggest that a greater reduction in scale dimensions or coverage on the wing membrane may entail higher costs in terms of hydrophobicity. However, large-scale comparative studies are currently lacking.

To fill that gap in our knowledge, here we explore to what extent anti-wetting ability is influenced by micro and nanostructure in species that largely differ in their wing microstructure, by selecting a subset of 23 species (Figure 3) from a broad study of 123 clearwing Lepidoptera species (30). In these species,

114 we explored the links between structure, hydrophobicity and optics while controlling for phylogenetic
115 relatedness between species. First, we explored the relationships between hydrophobicity and wing
116 structure, at macro-, micro- and nano-structural level: (i) we measured the contact angle (CA) made
117 by water droplets of various sizes on the wing (ii) We then quantified wing macro-, micro-, and nano-
118 structures, and related them to hydrophobicity. (iii) Using a modelling perspective, we ran various
119 Cassie-Baxter and Wenzel models differing by their assumptions and compared the predicted to the
120 observed CA values to assess the relative importance of microstructure and nanostructures in
121 determining the observed hydrophobicity. Second, to identify the selective pressures acting on
122 hydrophobicity, we tested whether hydrophobicity and light transmission showed potential trade-off
123 or synergy. If microstructures play a dominant role in conferring hydrophobicity, species most efficient
124 at transmitting light – which lack scales or have highly modified scales in low coverage on the wing
125 surface – are expected be less efficient at repelling water. Third, to identify whether hydrophobicity is
126 influenced by environmental conditions, we tested the links between habitat latitude and
127 hydrophobicity: if repelling water is more important in the tropics where rain and humidity are
128 inescapable, tropical species are expected to show higher hydrophobicity than temperate species.
129

130 **RESULTS**

131 **Variation in hydrophobicity and relation to wing macrostructure**

132 We measured the contact angle of water droplets and wing surface in the transparent and opaque
133 zones of the forewing of three museum specimens per species, and we monitored contact angle at
134 three times, as water evaporated and droplet size decreased (Figures 2 and S1). We performed classic
135 mixed models and Bayesian models, the latter controlling for species phylogenetic relatedness, to
136 explore to what extent hydrophobicity depends on general wing macrostructure (opaque and
137 transparent zone, wing area, shape). Comparing models controlling or not for phylogeny helped us
138 purge our results from spurious correlations arising from phylogenetic ancestry.

139 We observed a general decrease in hydrophobicity with water evaporation in the opaque zone
140 and in the transparent zone (Figure 4A). Transparency appeared costly: (i) the transparent zone
141 showed lower hydrophobicity than the opaque zone of the same wing, whatever the size of the water
142 droplet considered (Figure 4A, zone effect in Table S1, see Figure S2 for distribution of hydrophobicity
143 levels), (ii) and we observed a stronger decrease in hydrophobicity with water evaporation in the
144 transparent than in the opaque zone of the same wing (time x zone effect in mixed models in Table S1,
145 Figure 4A). CA did not correlate to wing length but negatively correlated to the Wing Area / Body
146 Volume ratio (Table S1, effect only important when correcting for phylogeny, Figure 4C). Contrary to
147 our expectation, species with more elongated wings (higher FW ratio) had a slightly lower
148 hydrophobicity (Figure 4C, effect marginally important when corrected for phylogeny in Table S1).

149 Finally, species with more elongated wings or with shorter wings exhibited a greater loss of
150 hydrophobicity with evaporation (LWratio x time effect in Table S1).

151 **Variation in hydrophobicity and relation to wing microstructure**

152 We used the same approach (classic mixed and Bayesian models) to explore to what extent
153 hydrophobicity depends on wing microstructure – namely scale presence, type (piliform and/or
154 lamellar), insertion (erect or flat on the wing membrane), coloration (transparent or coloured), and
155 density in both the transparent and the opaque zones – and wing scale nanostructures – namely the
156 width and spacing of longitudinal ridges that were present on all scales.

157 The influence of wing microstructure on hydrophobicity was pervasive in our results (Figure
158 5): (i) we found a higher interspecific variance in contact angle values in the transparent than in the
159 opaque zone (Figure 4A, Fligner-Killeen tests with all times together χ^2=79.48, p<0.001 or separated
160 at T1: χ^2=49.57, p<0.001; T2: χ^2=29.24, p<0.001; T3 χ^2=26.47, p<0.001), maybe in relation to the higher
161 interspecific microstructural diversity of the transparent zone. (ii) The nude membrane (N) yielded a
162 lower hydrophobicity (Scale presence effect shown in classic models in Table S3a, Scale Nb (0>1) effect
163 in classic and Bayesian models in S3b) but a similar decrease in hydrophobicity compared to the
164 structural strategies that involved scales (Table S2, scale presence effect in Table S3a, Figure 5). (iii)
165 Combining two types of scales (piliform and lamellar) yielded comparable levels of hydrophobicity, but
166 a lower decrease in hydrophobicity with evaporation than having only one type of scales only (Table
167 S2, Scale Nb (2>1) x Time interaction in Table S3b, Figure 5). (iv) The decrease in hydrophobicity with
168 evaporation was lower for erect coloured scales than for erect transparent scales (Table S2, Colour
169 EC>ET x Time interaction in Table S3c, Figure 5). (v) The decrease in hydrophobicity with water
170 evaporation was attenuated for denser scales (Table S2, time x density interaction in Table S3c, Figure
171 4B). This attenuation by density was stronger in the transparent zone than in the opaque zone (Table
172 S2, time x density x zone interaction in Table S3a, S3b, S3d, Figure 4B), and for erect scales (Table S2,
173 time x density interaction in Table S3c). (vi) For flat lamellar scales, the decrease in hydrophobicity with
174 evaporation was attenuated when scales were arranged in a higher number of layers, be they in the
175 transparent or in the opaque zone (Table S2, time x nb layers interaction in Table S3d). (vii) Finally,
176 scale nanostructures did not explain an important part of the variation in hydrophobicity (scale ridge
177 ratio never retained in the best models).

178 Because erect geometries (involving piliform and/or lamellar scales: PLE, PE, LE) appear to
179 behave differently in reaction to water than flat geometries, we analysed scale dimensions and spacing
180 by performing classic mixed models and Bayesian analyses on the broad dataset of 123 species used
181 by Gomez et al. (30) to get more representative trends. Compared to flat scales, erect scales were
182 shortened when one type of scale was involved, especially in lamellar scales (Figure S3, Table S4).
183 When both present, piliform and lamellar scales were in similar densities, close in space, and piliform

184 scales were 2.6 times longer than lamellar scales, creating a multi-hierarchical roughness at
185 microscopic scales (see SI for supplementary results, Table S4, Figure S4).

186 For modelling, we first assigned water droplets at T1 to a Cassie-Baxter regime when droplets
187 showed a high contact angle after evaporation (CA≥120° at T3; results remained the same when
188 shifting the threshold to 110°); otherwise, water droplets at T1 were assigned to a Wenzel regime
189 (CA<120° at T3). We tested Cassie-Baxter models with microstructures alone (scale dimensions,
190 insertion, and density) or with scale microstructures and nanostructures (ridge-ratio) to assess their
191 relative importance in determining hydrophobicity observed at T1, selecting as best the model that
192 minimized the difference between predictions and observations, for each structural strategy
193 separately (SI, Figure S5 for model details, Figure S6 for best model selection).

194 The best model included only microstructures for all erect strategies (with piliform and/or
195 lamellar scales PE, LE, PLE, with a mean difference between observations and predictions of 7°, 14°,
196 and 7° respectively) and for flat lamellar scales in low densities (not fully covering the wing membrane,
197 with a mean difference between observations and predictions of 22° and 25° for the transparent and
198 the opaque zone respectively). This was consistent with the fact that in these cases water contacted
199 scale contour/edge, which did not exhibit any nanostructures. For strategies involving erect piliform
200 scales (PE, PLE), the model with bending piliform scales outperformed the model with fully erect
201 piliform scales. For flat piliform scales (PF) and for flat lamellar scales (LF) in high densities (fully
202 covering the membrane), the best model included microstructures and scale nanostructures (with a
203 mean difference between observations and predictions of 9° for PF, 22° and 25° for LF for the
204 transparent and the opaque zone respectively). In this case, the scale upper side is in contact with
205 water and both types of structures come into play. In general, predictions were rather close to
206 observations with no systematic bias towards under or over-estimation of Φ_S, the fraction of the
207 droplet contact area where water is in contact with the solid (Figure 6).

208 For the water droplets not categorized as in a Cassie-Baxter state, we tested whether a Wenzel
209 model with microstructures only could predict the observed values at T1 (Figure S7). We could not test
210 a Wenzel model with micro and nanostructures, as it required to precisely characterize scale
211 nanogroove height and membrane nanostructures, which was not allowed on museum specimens.
212 Predictions of Wenzel models were far below observations (Figure S8).

213

214

215 **DISCUSSION**

216 We here considered hydrophobicity as a proxy for self-cleaning ability. Indeed, although we could not
217 quantify water droplet roll-off angles precisely with our set-up, we observed that water droplets rolled

218 off extremely fast from the wings when not perfectly horizontal (D Gomez & M Elias personal
219 observation July 2016; J Pairraire personal observation May 2018; C Houssin personal observation April
220 2021), which made our measurements particularly time-consuming. This suggested small roll-off
221 angles and weak water adhesion. Small roll-off angles are commonly found in opaque butterflies (15,
222 28) and in *Parantica sita* and *Parnassius glacialis*, the two clearwing butterfly species studied to date
223 (29).

224 The observed decrease in hydrophobicity with water evaporation is commonly observed in
225 hydrophobic human-made surfaces (14, 39, 40) and in natural surfaces, as in the transparent-winged
226 damselfly *Ischnura heterosticta* (3). It is interpreted as a loss of self-cleaning ability when contact angle
227 values get below the hydrophilicity threshold (3). Beyond this general trend, the lower hydrophobicity
228 and the stronger loss in hydrophobicity with water evaporation in the transparent than in the opaque
229 zone undoubtedly show that transparency entails important costs in terms of hydrophobicity.

230

231 **Variation in hydrophobicity and relation to wing macrostructure**

232 Relationships between hydrophobicity and wing macrostructure were surprising, probably due to the
233 taxonomic level investigated. Our absence of relationship between CA and wing length contrasted with
234 Byun et al.'s (4) marginal positive correlation between these variables (study on 24 species, 10 insect
235 orders, wing length effect on CA, estimate=10.58±5.33, t=1.99, p=0.067), Wing shape was much more
236 diverse in Byun et al.'s dataset (LWratio: min=1.2, mean=3.6, max=9.3) than in ours (23 species, 1 insect
237 order), LWratio: min=1.8, mean=2.2, max=3.2) When restricting Byun's dataset to our maximal value
238 for LWratio, the effect disappeared (n=13 species, wing length estimate=2.42 ± 5.09, t=-0.47, p=0.652).
239 Our finding a negative correlation between CA and the ratio of wing area to body volume contrasted
240 with Wagner et al.'s (26) positive correlation between CA and the ratio of wing area to body mass (
241 study on 38 species from 14 insect orders, wing area/body mass ratio effect on CA: estimate=11.09 ±
242 3.75, t=2.96, p=0.007), When restricting Wagner et al's dataset to insects without elytra but with a
243 microstructured membrane (Odonata, Ephemeroptera, Lepidoptera, some Planipennia), the effect
244 disappeared (n=21 species (4 insect orders), estimate=0.15 ± 1.12, t=-0.14, p=0.895). Finally, the
245 negative correlation between forewing elongation and CA (Figure 4C) is surprising. Water droplets
246 exert higher moment force when further away from the butterfly body and should select for higher
247 hydrophobicity; yet, more elongated wings may already show higher elasticity that may already ensure
248 rapid droplet roll-off through movement, and offset the need for a higher hydrophobicity.

249

250 **Variation in hydrophobicity and relation to wing microstructure**

251 Going back to the physical theory behind hydrophobicity, several studies have shown that a
252 single-level structure does not necessarily guarantee a low water adhesion, even in the Cassie-Baxter
253 state (see references in 7). Introducing higher levels of hierarchy increases the robustness of a surface
254 hydrophobicity (8): it stabilizes the Cassie-Baxter state by dramatically decreasing the contact area
255 fraction (ratio of contact area to the total surface area of the structure) and thus the adhesion force of
256 water droplets, and by enlarging the energy difference between the Cassie-Baxter and the Wenzel
257 states. Hierarchical structures can be frequently found in plants and in animals. For instance, in the
258 water strider *Gerris remigis*, leg water resistance is due to the hierarchical structures of nano-grooved
259 microsetae, which prevents striders from being drowned under heavy rainfall (42). This likely explains
260 why, in our study, the combination of erect piliform scales and lamellar scales yields a lower loss of
261 hydrophobicity with evaporation than piliform or lamellar scales alone. Such geometries have a 3-level
262 roughness: (1) erect piliform scales bending over lamellar scales (piliform scales are 2.6 times longer
263 than lamellar scales and first in contact with water), (2) erect lamellar scales tightly associated in space
264 to piliform scales (similar density and close spacing), and (3) nanostructures on scales and on the wing
265 membrane. Hydrophobicity likely results from the combination of the complex geometry of erect
266 microstructures (which considerably reduces the proportion of the total surface in contact with water),
267 and the gain in mechanical resistance (gain in elasticity and resistance against breakage) of piliform
268 scales when bending against lamellar scales. The importance of elasticity of bending hair-like
269 microstructures has been found in several studies. In the Lady's mantle plant (*Alchemilla vulgaris*),
270 hairs are hydrophilic when measured individually, but they bend and coalesce into bundles when in
271 contact with water droplets; their elasticity results in a repulsive interaction between the droplet and
272 the plant surface, which maintains hydrophobicity (CA above 90°) (43). Likewise, in *Nasutitermes*
273 termits, large bending hairs and small micrasters (micraster wavelength was around 11,7 µm according
274 to our measurements taken on Figure 3C from 41) enable hydrophobicity (CA above 90°) in both rain
275 and mist conditions (44).
276 Increasing the density of microstructures does not significantly change hydrophobicity, but
277 leads to a lower loss of hydrophobicity with water evaporation, i. e., to a higher resistance to tiny water
278 droplets. This can be seen for all structural strategies (effect time x density) and for flat scales organized
279 in layers (effect time x number of layers). This is consistent with the fact that, during droplet
280 evaporation, the Cassie-Baxter regime is more robust for large microstructure density. Not only scale
281 architecture but also coloration can contribute to hydrophobicity. Erect scales show a lower loss of
282 hydrophobicity when pigmented than when transparent. In the transparent zone, coloured scales
283 exhibit colours ranging from pale yellow to brown and black. They are likely impregnated by melanin
284 pigments, which are known to be involved – for some biochemical forms – in cuticle sclerotization
285 (hardening) (45). Hence, the additional hardening conferred by pigments may increase their

286 mechanical resistance to deformation and may contribute to maintaining hydrophobicity, even when
287 evaporation occurs.

288 We found that scale nanostructures did not contribute significantly to wing hydrophobicity for
289 most structural strategies, except for flat lamellar scales fully covering the wing membrane and
290 organized in layers, in the transparent or in the opaque zone, and for flat piliform scales in the
291 transparent zone (Figure S6). Our results bring novel evidence for a major role of microstructures in
292 explaining large variations in hydrophobicity when diverse microstructures are considered. The rare
293 existing studies on the subject suggest a synergetic effect of scale nanostructures and microstructures
294 on enhancing surface hydrophobicity (experiments on one type of microstructure, namely flat lamellar
295 scales in opaque butterflies, in (15, 46) or hairs in the wing of the housefly *Musca domestica* (47);
296 theoretical modelling on one type of microstructure in (48)), or even a major role of nanostructures in
297 the overall variation (15, 47). Yet, these two analyses only examine one type of microstructure, thereby
298 potentially underestimating the importance of microstructures when more types of microstructures
299 are considered. Overlap in scales is assumed to help anisotropy in hydrophobicity (49). Here, we find
300 that it attenuates the loss of hydrophobicity with water evaporation, thereby maintaining self-cleaning
301 ability more efficiently.

302 Wing mechanical resistance is crucial for flight and geometries that limit protrusion height are
303 more resistant to breakage and less hydrophobic (50). Several of our results suggest scale height may
304 be limited: (i) erect piliform scales are likely bending over the membrane as shown by modelling. (ii)
305 When piliform scales are alone, they have similar height, be they flat or erect, maybe because they
306 bend easily, which may limit their sensitivity to breakage. (iii) Erect lamellar scales are shortened
307 compared to flat lamellar scales, which likely increases their resistance to breakage. (iv) Erect
308 transparent lamellar scales are densely packed, as shown in Gomez et al. (30), which can also increase
309 their mechanical resistance. Further experiments are needed to elucidate these aspects, and clarify
310 the role of nanostructures, as not only their presence, but their topography and its randomness have
311 been recently suggested to play a role in determining antiwetting properties (51).

312 Finally, the poor predictability of Wenzel model is not surprising since the validity of Wenzel
313 model – as currently formulated – is widely questioned in the literature (41 and references therein).
314 This is especially true for our dataset given that most microstructures only weakly increase the
315 roughness parameter r (see materials and methods) while providing strong pinning sites for the contact
316 line and thus significantly increasing the contact angle measured at T1.

317

318

319 **Trade-off between hydrophobicity and optical transparency**

320 Using spectrometric measurements of wing direct transmittance, we found a negative relationship

321 between contact angle and mean transmittance over 300-700 nm (Table S5, Figure 7). A 10% increase
322 in transmittance resulted in a 4° loss in CA. While this relationship was marginally significant without
323 controlling for phylogenetic relatedness, whatever the level of analysis (all CA values, mean CA values
324 per individual, mean CA values per species), it was statistically important (i. e., the 95% credibility
325 interval did not contain 0) in phylogeny-controlled analyses when considering all measurements or
326 mean individual values, but less important at species level (90% credibility interval), likely because of
327 weaker statistical power. In agreement with our prediction that microstructures play a major role in
328 hydrophobicity, we find a negative relationship between hydrophobicity and transparency, a condition
329 associated with major modifications in scale shape and density. This trade-off can be seen from the
330 literature: the nymphalid butterfly *Greta oto* has been shown to exhibit a high transparency resulting
331 from poorly dense erect piliform scales and efficient antireflective nanostructures (35, 37) but a weak
332 hydrophobicity (27). Likewise, the trade-off can be seen in the dragonfly *Gynacantha dravida* (which
333 has micro and nanospikes), in which distal wing parts show higher hydrophobicity but lower
334 transmittance compared to proximal wing parts (52). Finding this trade-off is fully compatible with the
335 fact that some species with nude membrane show high hydrophobicity: membrane nanostructures are
336 at full play in species with nude membrane and can potentially efficiently reduce both reflection and
337 water adhesion, like in the cicada *Aleeta curvicosta* (53). In species with erect scales, our models show
338 a major role of microstructures and a negligible role of nanostructures in hydrophobicity. If selection
339 for hydrophobicity is relaxed on membrane nanostructures in species with erect scales, this may
340 explain why nanostructures are so diverse in their architecture (type, density), as recently shown in
341 clearwing Lepidoptera (36).
342
343 **Hydrophobicity and latitude**
344 Compared to their temperate counterparts, species living in the tropics had a higher hydrophobicity in
345 their transparent zone – loss of 10° CA for 10° increase in latitude – but a similar hydrophobicity in
346 their opaque zone (Table S6, Figure 8) All species showed superhydrophobic opaque patches (intercept
347 above 150° in Table S6, Figure 8B) and there was no relationship between the proportion of wing area
348 occupied by transparency and latitude that could have explained the observed variations in CA (model
349 with proportion of transparency as dependent variable, latitude effect = 0.08 $\pm$ 0.22, t=-0.31, p=0.76,
350 the best model was the null model). This result is consistent with the prediction that in tropical climates
351 where species face more humid conditions, and where rainfall can happen daily, there is a stronger
352 selective pressure for increased hydrophobicity. While the opaque zone allows maximizing
353 hydrophobicity in all environmental conditions, the differential in environmental conditions reveals
354 the costs of transparency. To our knowledge, this is the first evidence for a higher hydrophobicity in
355 more humid conditions. Scarce relevant studies have explored the link between habitat humidity and

species hydrophobicity: at local geographical scale, all four cicada species studied by (6) show superhydrophobicity regardless of whether they live in dry or more humid habitats, but annual species are more hydrophobic than the species that emerges in large swarms every 17 years. Likewise, Goodwyn et al. (29) suggest that in transparent butterflies hydrophobicity may depend on lifespan and migration ability. Further studies are needed to elucidate the links between hydrophobicity and species ecology.

This study is the first to mix many architectures at microscale and give access to the relative role of micro and nanostructures at transmitting light and repelling water. It shows that selection likely acts on multiple features of scales (shape, orientation, coloration, density) in relation to climatic conditions. Considering more natural geometric complexity in experimental and theoretical studies on hydrophobicity should open new venues for applied physics and answer open questions like the role of randomness in nanostructures, shown to improve optical transparency (35) but suggested to impair hydrophobicity (54, but see 51).

MATERIALS AND METHODS

Species selection

Scale type and scale insertion have been suggested to influence hydrophobicity(29); scale coloration, often involving melanin deposition which increases cuticle hardening in insects (45), could increase scale stiffness and ability to repel water droplets. Hence, we selected a set of species varying in structural strategies – scale type (N=nude membrane, P=piliform bifid or monofid scales, L=shape different than piliform, hereafter called lamellar, or PL=association of piliform and lamellar scales), insertion (E=erect or F=flat), and colouration (C=coloured or T=transparent) – from the study of 123 species of clearwing Lepidoptera (30). We minimized the phylogenetic relatedness between species harbouring the same type of structural strategies to increase the power of comparative analyses. We selected a total of 23 species from 10 families (Figure 1 & 2, list in Table S7), comprising 3 species for the structural strategies (N, PFC, PEC, LFC, LFT, LEC, LET), 2 species for PLEC and LEC, and 1 species for PLET, as for some species only a limited number of specimens were present in the collections. For each species, we selected three specimens in good condition either from Paris MNHN collections or from our own private collections. 54/69 specimens (all species but *Eutresis hypereia*) had labels with exact collect location that could be tracked down to GPS coordinates.

Hydrophobicity measurements

391 For each specimen, we used a purpose-built water-droplet dispenser (a graduated pipette on a holder)
392 and a Keyence VHX-5000 microscope (equipped with Z20 zoom) to image water droplets on butterfly
393 wings. As a general procedure, we dropped a series of three 1µl water droplets (volume usually taken
394 to assess hydrophobicity (3, 29)) at three locations of the transparent and opaque zones of the dorsal
395 side of a wing. After the water droplet was dropped (time T1), we allowed its volume to be
396 approximately divided by two (time T2) and by four (time T3) compared to its original volume. Since
397 evaporation kinetics depended on droplet shape, time intervals elapsed between consecutive photos
398 were not identical from one species to another. At each time, we took a photo (Figure 1) in which we
399 measured the static contact angle (Figure S1). Contact angle measurements were first measured on
400 both wings and found highly repeatable (see detailed methods and results in SI, Table S8). We thus
401 kept the same protocol, but we measured only the forewing.
402
403 **Measurements of wing macro, micro and nanostructure**
404 To characterize wing macrostructure, we took photos of the three specimens of each species using a
405 camera (D800E Nikon, 60mm lens, annular light). We analysed photos using ImageJ (55). Given the role
406 of wing length (4), maybe wing shape (4), and ratio of total wing area to body mass (53) on
407 hydrophobicity and self-cleaning ability, we computed wing length, length-to-width LW ratio and the
408 ratio of total wing area to body volume, taking the volume as a proxy for mass for dry specimens, and
409 assuming the body to be a cylinder, for which we measured length (thorax+abdomen) and width. Using
410 the 'rptR' package (56), we found that all wing macrostructural measurements were repeatable, i.e.
411 that a specimen was representative of its species for all wing macrostructural variables (Table S8).
412 To characterize wing microstructure (i.e. scale characteristics, presence, type, insertion,
413 coloration, density), we imaged the dorsal side of forewing transparent and opaque zones using
414 microscopes (Zeiss Stereo Discovery V20 and Keyence VHX-5000). We did that in one specimen per
415 species because scale dimensions and density had already been found repeatable at zone by species
416 level in Gomez et al. (30). Using ImageJ or the Keyence built-in tool, we measured scale density (per
417 mm^2), length and width (µm), scale surface (in μm^2) as the product of length by width, and scale
418 coverage as the product of scale surface (expressed in mm^2) by scale density. We counted the number
419 of different scale types: 0=nude membrane, 1= lamellar scales or piliform scales, 2= combination of
420 piliform scales and lamellar scales. For flat lamellar scales, we also computed the density of scale top
421 layer and computed the number of layers as the ratio between density and top layer density.
422 We quantified scale nanostructures – width and spacing (in µm) of longitudinal ridges
423 present on all scales – on the detailed top-view microscopical images. We computed the ridge-ratio as
424 ridge width to spacing (SI, Fig S2). Since museum specimens are patrimonial material, we could not
425 damage or destroy specimens to image membrane nanostructures or scale ridge height.

426

427 **Optical measurements**

428 For one specimen per species, we measured specular transmittance from 300 to 700 nm as in Gomez
429 et al. (30), using a deuterium-halogen lamp (Avalight DHS), direct optic fibres (FC-UV200-2-1.5 x 100)
430 and a spectrometer (Avaspec-2048 L, Avantes). Wing samples were placed perpendicular at equal
431 distance between fibres aligned 5 mm apart (1 mm diameter spot). We took five measurements of the
432 forewing in various points of the transparent zone. Using Avicol v6 (57), we computed the mean
433 transmittance over [300-700] nm, which described the level of optical transparency. Optical
434 measurements had been found highly repeatable at species level in Gomez et al. (30).

435

436 **Comparative analyses**

437 All analyses were conducted using the R environment_(58)._We conducted mixed models not
438 controlling for phylogeny using the 'nlme' R package (59). We selected the best mixed model using
439 AICc minimization. We used the formulated model for Bayesian mixed models with MCMC analyses
440 controlling for phylogeny, using the 'mulTree' R package (60). Bayesian analyses used the maximum
441 clade credibility (MCC) phylogeny obtained in Gomez et al. (30) and pruned to targeted species.
442 Comparing classic and Bayesian mixed models allowed us to assess the influence, if any, of phylogeny
443 on the observed relationships. For Bayesian analyses, we used uninformative priors, an Inverse-
444 Gamma distribution (shape = 0.001, scale = 0.001) for both random effect and residual variances (61),
445 2 chains of 500,000 iterations, burn-in of 10,000, and thinning interval of 300. Fixed effects were
446 considered statistically important when associated with 95% credibility intervals excluding zero, and
447 less important (marginally important) when associated with 90% credibility interval excluding zero.

448 Considering all contact angle measurements, we analysed the variation in contact angle with
449 (i) wing macrostructure descriptors – time, zone, forewing size, surface, LW ratio, the ratio of total
450 wing area divided by body volume, and relevant two and three-way interactions –; (ii) with wing
451 microstructure descriptors – time, zone, wing length (to correct for variation in scale dimensions), scale
452 length, width, density, scale type, number of different types, scale insertion, scale colouration, number
453 of layers, ridge-ratio, and biologically relevant two and three-way interactions. (iii) To characterize
454 spatial geometries, we analysed scale length against scale insertion for structural strategies with one
455 scale type. For structural strategies based on both scale types (piliform and lamellar), we analyzed
456 length ratio, density ratio and spatial association between the two scale types in relation to scale
457 insertion (see SI for details). (iv) We analyzed the difference between contact angles predicted by
458 various Cassie-Baxter and Wenzel models (see below) and measured contact angles at T1 to select the
459 best models. (v) We tested for a potential trade-off between optical transparency and wing
460 hydrophobicity, considering all measurements of contact angle, individual mean values, or species

461 mean values at T1. (vi) Finally, we tested whether tropical species were more hydrophobic than
462 temperate species. To do so, we related for each specimen its average CA value to its latitude to the
463 equator, the proportion of wing area occupied by transparency and wing length, while taking species
464 as random effect, for the opaque and transparent zone separately. We also tested whether variation
465 in the proportion of transparency could be explained by the latitude to the equator.
466
467 **Hydrophobicity modelling**
468 To assess to what extent scale micro- and nanostructure could explain the observed variation in
469 hydrophobicity, we elaborated Cassie-Baxter model (62), whereby water only wets the top of the
470 surface and the apparent contact angle observed at equilibrium is θ^*.

471 $$\cos\theta^* = \Phi_S \cos\theta_S + \Phi_A \cos\theta_A \text{.....(Eq 1)}$$

472 where Φ_S is the fraction of the droplet contact area where water is in contact with the solid, and Φ_A
473 is the fraction of droplet contact area in contact with air, with $\Phi_S + \Phi_A = 1$. $\theta_A = 180°$ (contact angle
474 of water with air) and the angle θ_S (also called Young angle) is the contact angle of water on an ideal
475 smooth surface of the same material (wing membrane), set to 95°, as in Fang et al (15), a plausible
476 value given the presence of epicuticular wax on the wing membrane (63), even in clearwing
477 Lepidoptera (37). This equation is valid for water droplet size largely exceeding surface roughness
478 wavelength (64), which is the case for 1µl water droplets. Considering flat-topped geometries
479 simplifies Eq1 to:

480 $$\cos\theta^* = \Phi_S \cos\theta_S - (1 - \Phi_S) \text{.....(Eq 2)}$$

481 While $\Phi_S = 1$ for a nude membrane, $\Phi_S < 1$ for all the other microstructures (Figure S5 for
482 calculations). We explored several hypotheses: piliform scales fully erect or bending over a fraction pp
483 = 3/5 of their length (the value 3/5 comes from P/L length ratio = 2.6 found for PLE strategies in Figure
484 S4), an organization of flat lamellar scales in one layer if in low density, or several layers (NL) when in
485 high density, models with microstructures only, or with micro and nanostructures. In the latter case,
486 we considered water droplets contacted scale nanostructures whether flat scales (PF or LF) covered
487 the wing membrane entirely or not, or only when scales were in high coverage, building a
488 homogeneous horizontal surface.
489 We also elaborated a Wenzel model (1), whereby water fills all the pores of the surface and
490 the wetting contact angle is primarily determined by surface roughness r. The apparent contact angle
491 θ^* is obtained by:

492 $$\cos\theta^* = r \cos\theta_S \text{.....(Eq 3)}$$

493 where r is the ratio between the total solid surface and the projected surface, and the angle θ_S is the
494 same as previously. We only included microstructures in the model since we had no measurement of
495 scale ridge height or membrane nanostructures. While r=1 for a nude membrane, r exceeds 1 for all

the other microstructures (see Figure S7 for calculations).

ACKNOWLEDGEMENTS

We warmly thank Jacques Pierre and Rodolphe Rougerie for help with species choice, identification, and data on species ecology, Edgar Attivissimo for contributing to Keyence imaging, and Thibaud Decaëns, Daniel Herbin, and Claude Tautel for species selection and identification.

COMPETING INTERESTS

This work was funded by Clearwing ANR project (ANR-16-CE02-0012), HFSP project on transparency (RGP0014/2016) and a France-Berkeley fund grant (FBF #2015-58). No competing interest. The authors declare no competing interests.

AUTHOR CONTRIBUTIONS

Doris Gomez study and protocol design, funding acquisition, specimen selection, macrostructure and microstructure measurements, optical measurements, data curation and analysis, hydrophobicity modelling, writing original draft. Jonathan Pairraire: protocol design, structure and CA measurements, CA computation. Charline Pinna: protocol design. Monica Arias: hydrophobicity modelling. Celine Houssin: protocol design, structure and CA measurements, CA computation. Jerome Barbut: species selection. Serge Berthier: study design, funding acquisition, writing review and editing. Christine Andraud: study and protocol design, writing, funding acquisition, writing review and editing. Thierry Ondarçuhu: hydrophobicity modelling, writing review and editing, Conceptualization. Marianne Elias: study and protocol design, funding acquisition, specimen selection, data curation and analysis, writing review and editing.

DATA AND CODE AVAILABILITY

Data are available at: https://doi.org/10.17605/OSF.IO/GB49E

Code availability: upon manuscript acceptance in a journal

ORCIDS

Doris Gomez http://orcid.org/0000-0002-9144-3426
Charline Sophie Pinna http://orcid.org/0000-0002-4947-0893
Monica Arias: http://orcid.org/0000-0003-1331-2604
Christine Andraud http://orcid.org/0000-0002-3112-9363
Serge Berthier http://orcid.org/0000-0002-9255-059X
Thierry Ondarçuhu: http://orcid.org/0000-0001-7657-5271
Marianne Elias http://orcid.org/0000-0002-1250-2353

533

534

535 **REFERENCES**

536

537 1. R. N. Wenzel, Resistance of solid surfaces to wetting by water. *Ind. Eng. Chem.* **28**, 988–994
538 (1936).
539 2. W. Barthlott, C. Neinhuis, Purity of the sacred lotus, or escape from contamination in biological
540 surfaces. *Planta* **202**, 1–8 (1997).
541 3. J. Hasan, *et al.*, Spatial Variations and Temporal Metastability of the Self-Cleaning and
542 Superhydrophobic Properties of Damselfly Wings. *Langmuir* **28**, 17404–17409 (2012).
543 4. D. Byun, *et al.*, Wetting Characteristics of Insect Wing Surfaces. *J. Bionic Eng.* **6**, 63–70 (2009).
544 5. M. Sun, G. S. Watson, Y. Zheng, J. A. Watson, A. Liang, Wetting properties on nanostructured
545 surfaces of cicada wings. *J Exp Biol* **212**, 3148–3155 (2009).
546 6. J. Oh, *et al.*, Exploring the Role of Habitat on the Wettability of Cicada Wings. *ACS Appl. Mater.*
547 *Interfaces* **9**, 27173–27184 (2017).
548 7. Y. Su, *et al.*, Nano to Micro Structural Hierarchy Is Crucial for Stable Superhydrophobic and Water-
549 Repellent Surfaces. *Langmuir* **26**, 4984–4989 (2010).
550 8. M. S. Bell, A. Shahraz, K. A. Fichthorn, A. Borhan, Effects of Hierarchical Surface Roughness on
551 Droplet Contact Angle. *Langmuir* **31**, 6752–6762 (2015).
552 9. W. Barthlott, M. Mail, C. Neinhuis, Superhydrophobic hierarchically structured surfaces in
553 biology: evolution, structural principles and biomimetic applications. *Philos. Trans. R. Soc. A-*
554 *Math. Phys. Eng. Sci.* **374**, 20160191 (2016).
555 10. N. A. Patankar, Mimicking the lotus effect: Influence of double roughness structures and slender
556 pillars. *Langmuir* **20**, 8209–8213 (2004).
557 11. F. Porcheron, P. A. Monson, Mean-Field Theory of Liquid Droplets on Roughened Solid Surfaces:
558 Application to Superhydrophobicity. *Langmuir* **22**, 1595–1601 (2006).
559 12. W. Ding, M. Fernandino, C. A. Dorao, Conical micro-structures as a route for achieving super-
560 repellency in surfaces with intrinsic hydrophobic properties. *Appl. Phys. Lett.* **115**, 053703 (2019).
561 13. C. E. Cansoy, H. Y. Erbil, O. Akar, T. Akin, Effect of pattern size and geometry on the use of Cassie–
562 Baxter equation for superhydrophobic surfaces. *Colloids and Surfaces A: Physicochemical and*
563 *Engineering Aspects* **386**, 116–124 (2011).
564 14. P. Tsai, R. G. H. Lammertink, M. Wessling, D. Lohse, Evaporation-Triggered Wetting Transition for
565 Water Droplets upon Hydrophobic Microstructures. *Phys. Rev. Lett.* **104**, 116102 (2010).
566 15. Y. Fang, G. Sun, Y. H. Bi, H. Zhi, Multiple-dimensional micro/nano structural models for
567 hydrophobicity of butterfly wing surfaces and coupling mechanism. *Sci. Bull.* **60**, 256–263 (2015).

16. A. Sanchez-Monge, J. Rodriguez Arrieta, M. Jimenez-Chavarria, A. Retana-Salazar, Observations on the Ultrastructure and Hydrophobicity of the Wings of Thirteen Neotropical Families of Diptera (insecta) with Comments on Their Flight. *Acta Microsc.* **24**, 111–117 (2015).
17. I. N. Miaoulis, B. D. Heilman, Butterfly thin films serve as solar collectors. *Ann. Entomol. Soc. Am.* **91**, 122–127 (1998).
18. I. C. Cuthill, *et al.*, Disruptive coloration and background pattern matching. *Nature* **434**, 72–74 (2005).
19. M. Stevens, C. L. Stubbins, C. J. Hardman, The anti-predator function of "eyespots" on camouflaged and conspicuous prey. *Behav. Ecol. Sociobiol.* **62**, 1787–1793 (2008).
20. D. J. Kemp, Female butterflies prefer males bearing bright iridescent ornamentation. *Proc Royal Soc B* **274**, 1043–1047 (2007).
21. S. Berthier, Thermoregulation and spectral selectivity of the tropical butterfly *Prepona meander*: a remarkable example of temperature auto-regulation. *Appl Phys A-Mater* **80**, 1397–1400 (2005).
22. A. Krishna, *et al.*, Infrared optical and thermal properties of microstructures in butterfly wings. *Proc Natl Acad Sci USA* **117**, 1566–1572 (2020).
23. C.-C. Tsai, *et al.*, Physical and behavioral adaptations to prevent overheating of the living wings of butterflies. *Nat Commun* **11**, 551 (2020).
24. W. Nachtigall, Aerodynamische Messungen am Tragfluegelsystem segeinder Schmetterlinge. *Journal of Comparative Physiology A* **54**, 210–231 (1967).
25. N. Slegers, *et al.*, Beneficial aerodynamic effect of wing scales on the climbing flight of butterflies. *Bioinspir. Biomim.* **12**, 016013 (2017).
26. T. Wagner, C. Neinhuis, W. Barthlott, Wettability and contaminability of insect wings as a function of their surface sculptures. *Acta Zoologica* **77**, 213–225 (1996).
27. N. D. Wanasekara, V. B. Chalivendra, Role of surface roughness on wettability and coefficient of restitution in butterfly wings. *Soft Matter* **7**, 373–379 (2011).
28. Y. Fang, *et al.*, "Micro-morphological Models for the Special Wettability of Locust and Moth Wing" in *Proceedings of the 2017 5th International Conference on Mechatronics, Materials, Chemistry and Computer Engineering (Icmmcce 2017)*, M. Wang, X. Zhou, Eds. (Atlantis Press, 2017), pp. 330–333.
29. P. Perez Goodwyn, Y. Maezono, N. Hosoda, K. Fujisaki, Waterproof and translucent wings at the same time: problems and solutions in butterflies. *Naturwissenschaften* **96**, 781–787 (2009).
30. D. Gomez, *et al.*, Transparency in butterflies and moths: structural diversity, optical properties and ecological relevance. *Ecological Monographs* (2021) https:/doi.org/10.1101/2020.05.14.093450 (May 19, 2020).
31. M. McClure, *et al.*, Why has transparency evolved in aposematic butterflies? Insights from the

603 largest radiation of aposematic butterflies, the Ithomiini. *Proc Royal Soc B* **286**, 20182769 (2019).
604 32. M. Arias, *et al.*, Transparency reduces predator detection in chemically protected clearwing
605 butterflies. *Funct Ecol* (2019) https:/doi.org/10.1111/1365-2435.13315.
606 33. M. Arias, M. Elias, C. Andraud, S. Berthier, D. Gomez, Transparency improves concealment in
607 cryptically coloured moths. *J Evol Biol* **33**, 247–252 (2020).
608 34. A. Yoshida, M. Motoyama, A. Kosaku, K. Miyamoto, Antireflective nanoprotuberance array in the
609 transparent wing of a hawkmoth, *Cephonodes hylas*. *Zoological Science* **14**, 737–741 (1997).
610 35. R. H. Siddique, G. Gomard, H. Holscher, The role of random nanostructures for the
611 omnidirectional anti-reflection properties of the glasswing butterfly. *Nature Communications* **6**
612 (2015).
613 36. C. Pinna, *et al.*, Convergence in light transmission properties of transparent wing areas in
614 clearwing mimetic butterflies. *bioRxiv*, 2020.06.30.180612 (2020).
615 37. A. F. Pomerantz, *et al.*, Developmental, cellular, and biochemical basis of transparency in the
616 glasswing butterfly Greta oto. *Journal of Experimental Biology* **accepted**, eb237917 (2021).
617 38. Y. M. Zheng, X. F. Gao, L. Jiang, Directional adhesion of superhydrophobic butterfly wings. *Soft*
618 *Matter* **3**, 178–182 (2007).
619 39. G. McHale, S. Aqil, N. J. Shirtcliffe, M. I. Newton, H. Y. Erbil, Analysis of Droplet Evaporation on a
620 Superhydrophobic Surface. *Langmuir* **21**, 11053–11060 (2005).
621 40. M. Reyssat, J. M. Yeomans, D. Quéré, Impalement of fakir drops. *EPL* **81**, 26006 (2007).
622 41. D. Quéré, Wetting and Roughness. *Annual Review of Materials Research* **38**, 71–99 (2008).
623 42. X. Gao, L. Jiang, Water-repellent legs of water striders: Biophysics. *Nature* **432**, 36–36 (2004).
624 43. A. Otten, S. Herminghaus, How Plants Keep Dry: A Physicist's Point of View. *Langmuir* **20**, 2405–
625 2408 (2004).
626 44. G. S. Watson, B. W. Cribb, J. A. Watson, Contrasting Micro/Nano Architecture on Termite Wings:
627 Two Divergent Strategies for Optimising Success of Colonisation Flights. *PLOS ONE* **6**, e24368
628 (2011).
629 45. M. Sugumaran, Complexities of cuticular pigmentation in insects. *Pigment Cell & Melanoma*
630 *Research* **22**, 523–525 (2009).
631 46. S. N. Aideo, D. Mohanta, Unusually diverse surface-wettability features found in the wings of
632 butterflies across Lepidoptera order and evaluation of generic and vertical gibbosity-based
633 models. *Phys. Scr.* **96**, 085004 (2021).
634 47. Q. Wan, *et al.*, Combination of active behaviors and passive structures contributes to the
635 cleanliness of housefly wing surfaces: A new insight for the design of cleaning materials. *Colloid*
636 *Surf. B-Biointerfaces* **180**, 473–480 (2019).
637 48. S. H. Sajadinia, F. Sharif, Thermodynamic analysis of the wetting behavior of dual scale patterned

638 hydrophobic surfaces. *Journal of Colloid and Interface Science* **344**, 575–583 (2010).
639 49. D. Bixler, B. Bhushan, Rice- and butterfly-wing effect inspired self-cleaning and low drag
640 micro/nanopatterned surfaces in water, oil, and air flow. *Nanoscale* **6**, 76–96 (2014).
641 50. E. Bittoun, A. Marmur, The Role of Multiscale Roughness in the Lotus Effect: Is It Essential for
642 Super-Hydrophobicity? *Langmuir* **28**, 13933–13942 (2012).
643 51. Y. Li, *et al.*, Biomimetic Random Arrays of Nanopillars and Nanocones with Robust Antiwetting
644 Characteristics. *J. Phys. Chem. C* **124**, 17095–17102 (2020).
645 52. S. N. Aideo, D. Mohanta, Limiting hydrophobic behavior and reflectance response of dragonfly
646 and damselfly wings. *Applied Surface Science* **387**, 609–616 (2016).
647 53. G. S. Watson, S. Myhra, B. W. Cribb, J. A. Watson, Putative functions and functional efficiency of
648 ordered cuticular nanoarrays on insect wings. *Biophys. J.* **94**, 3352–3360 (2008).
649 54. M. Sun, *et al.*, Influence of Cuticle Nanostructuring on the Wetting Behaviour/States on Cicada
650 Wings. *PLOS ONE* **7**, e35056 (2012).
651 55. C. A. Schneider, W. S. Rasband, K. W. Eliceiri, NIH Image to ImageJ: 25 years of image analysis.
652 *Nat. Methods* **9**, 671–675 (2012).
653 56. M. A. Stoffel, S. Nakagawa, H. Schielzeth, rptR: repeatability estimation and variance
654 decomposition by generalized linear mixed-effects models. *Methods Ecol Evol* **8**, 1639–1644
655 (2017).
656 57. D. Gomez, *AVICOL v6. a program to analyse spectrometric data. Free program available from the*
657 *author upon request at dodogomez@yahoo.fr or by download from*
658 *http://sites.google.com/site/avicolprogram/* (2011).
659 58. R Development Core Team, *R: a language and environment for statistical computing* (R
660 Foundation for Statistical Computing, 2013).
661 59. J. Pinheiro, D. Bates, D. DebRoy, D. R. Sarkar, nlme: linear and nonlinear mixed effects models. R
662 package version 3.1-145 (2020).
663 60. T. Guillerme, K. Healy, mulTree: performs MCMCglmm on multiple phylogenetic trees. R package
664 version 1.3.6. (2019).
665 61. J. D. Hadfield, MCMC methods for multi-response generalized linear mixed models: The
666 MCMCglmm *R* Package. *J Stat Soft* **33** (2010).
667 62. A. B. D. Cassie, S. Baxter, Wettability of porous surfaces. *Transactions of the Faraday Society* **40**,
668 546 (1944).
669 63. E. P. Ivanova, *et al.*, Molecular Organization of the Nanoscale Surface Structures of the Dragonfly
670 Hemianax papuensis Wing Epicuticle. *PLOS ONE* **8**, e67893 (2013).
671 64. A. J. B. Milne, A. Amirfazli, The Cassie equation: How it is meant to be used. *Advances in Colloid*
672 *and Interface Science* **170**, 48–55 (2012).

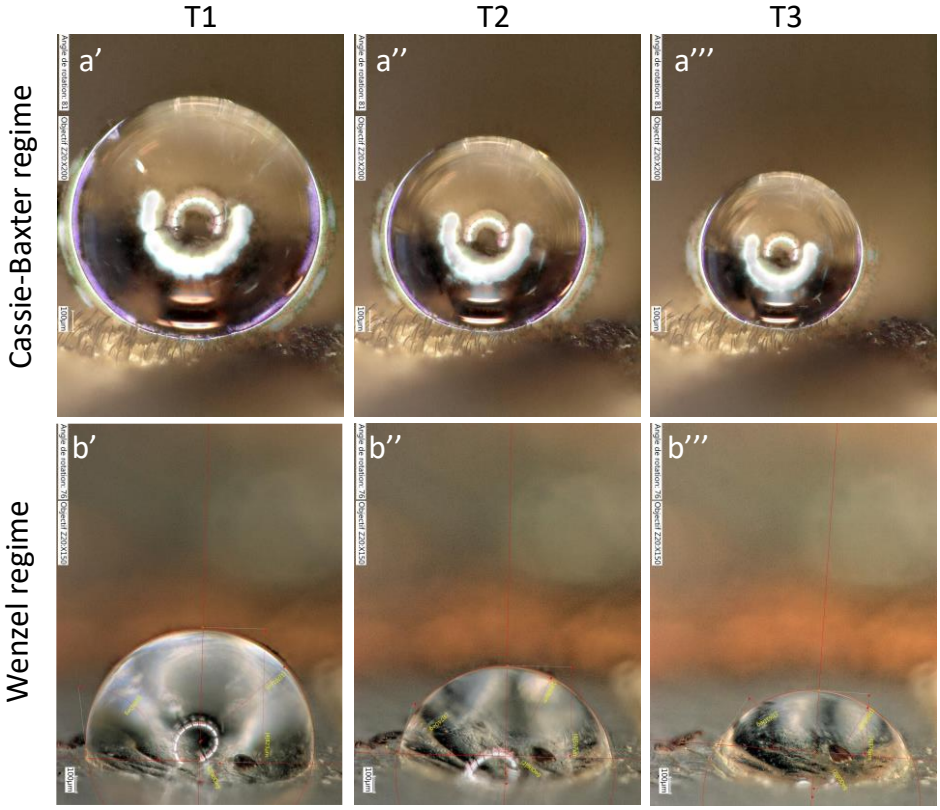

Figure 1. Examples of water droplets dropped in the transparent zone: Cassie-Baxter regime (series a) for *Eutresis hypereia* combining erected coloured piliform and lamellar scales and Wenzel regime (series b) for *Neorcarnegia basirei* with a nude membrane. Water droplet evolution is shown at different times: T1 (a', b'), T2 (a'', b''), and at T3 (a''', b''').

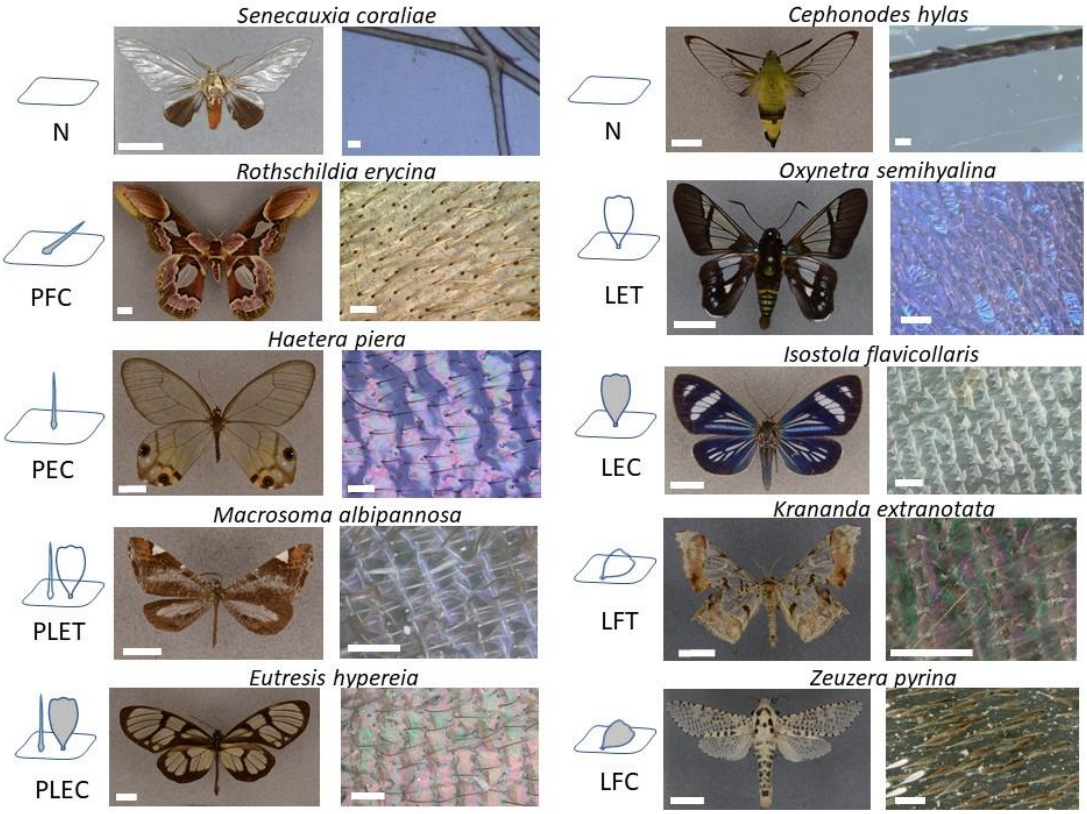

Figure 2. Examples of structural strategies in clearwing butterflies. Structural strategy is a combination of scale type (N: no scales, P: piliform scales, L: lamellar scales, PL: combination of piliform scales and lamellar scales), scale insertion (E: erected, and F: flat), and scale colour (C: coloured, and T: transparent). Notice that *Macrosoma albipannosa* has transparent lamellar scales but coloured piliform scales.

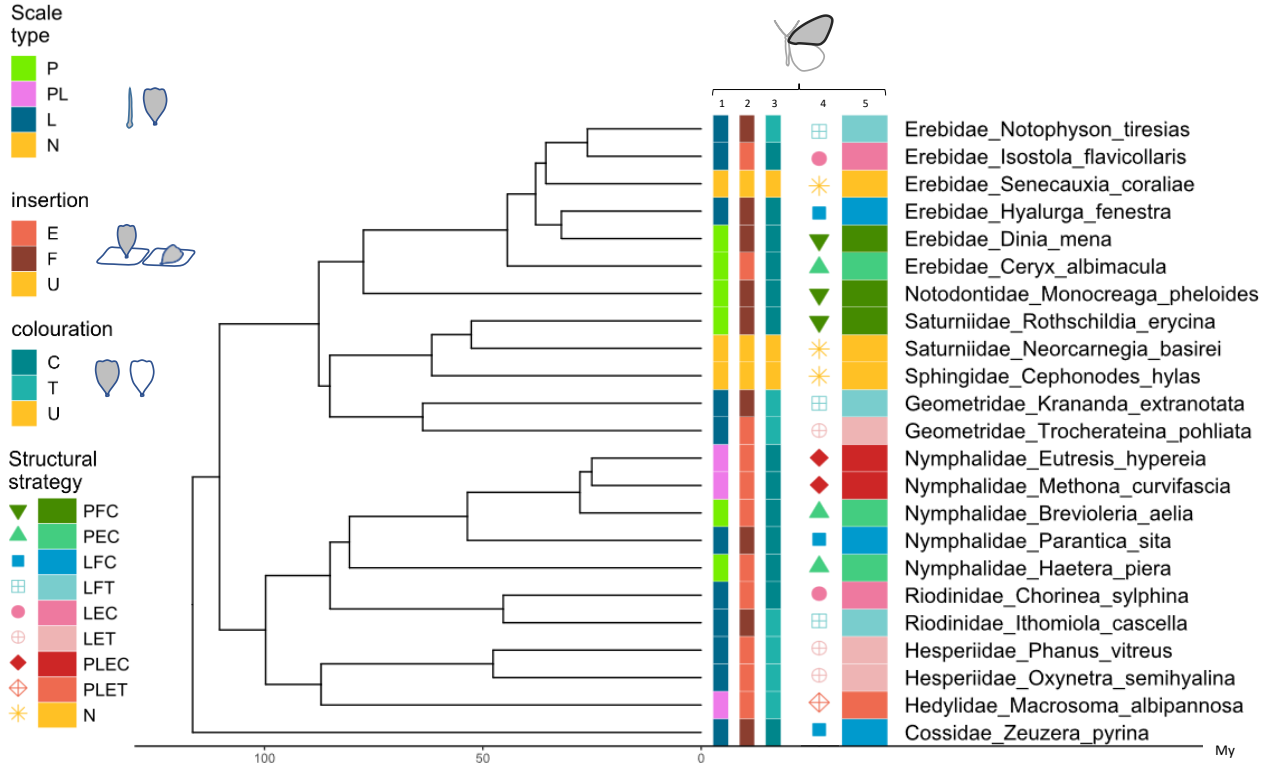

Figure 3. Phylogeny and distribution of trait values in the study species, for the forewing. Scale type (column 1), scale insertion on the membrane (column 2), scale colouration (column 3), and structural strategy (columns 4 and 5). For scale type: N=no scales, P=piliform scales, L= lamellar scales PL=combination of piliform scales and lamellar scales. For scale insertion on the membrane: E=erected, F=flat, U=undefined (for absent scales). For scale colouration: C=coloured, T=transparent, U=undefined (for absent scales). The strategy NUU was simplified into N.

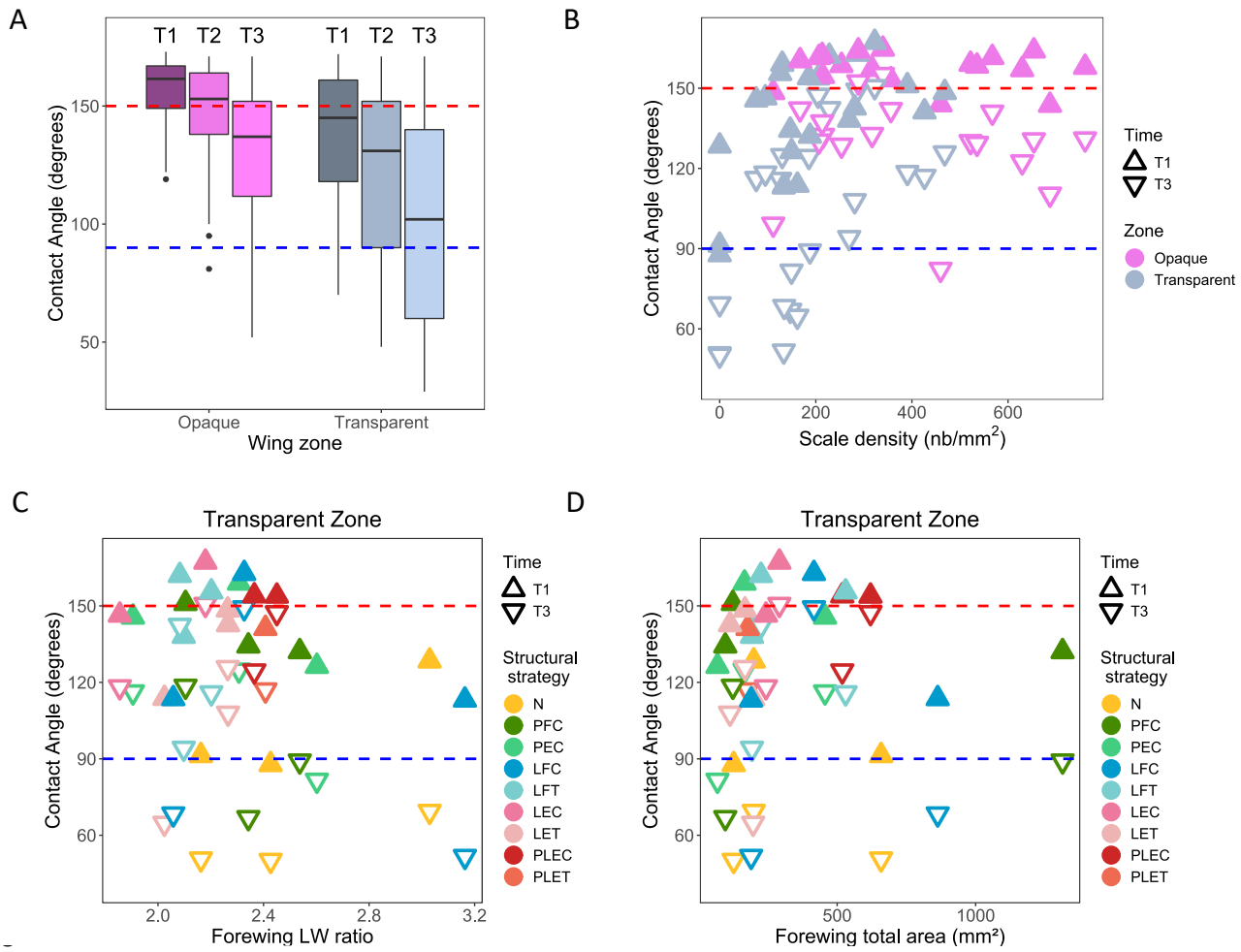

Figure 4. Variation in contact angle with evaporation time(A) and with scale density (B) in the transparent and opaque zones. Variation in contact angle with forewing length-to-width ratio (C) and total area (D) in the transparent zone. Structural strategy is a combination of scale type (N: no scales, P: piliform scales, L: lamellar scales, PL: combination of piliform scales and lamellar scales), scale insertion (E: erected, and F: flat), and scale colour (C: coloured, and T: transparent). Superhydrophobic: >150° (above the red line), hydrophobic: <150° and >90°; hydrophilic: <90° (below the blue line). (A) all measurements considered, (BCD) mean CA values for each species, zone, and time. Results are presented in Tables S1 to S3d.

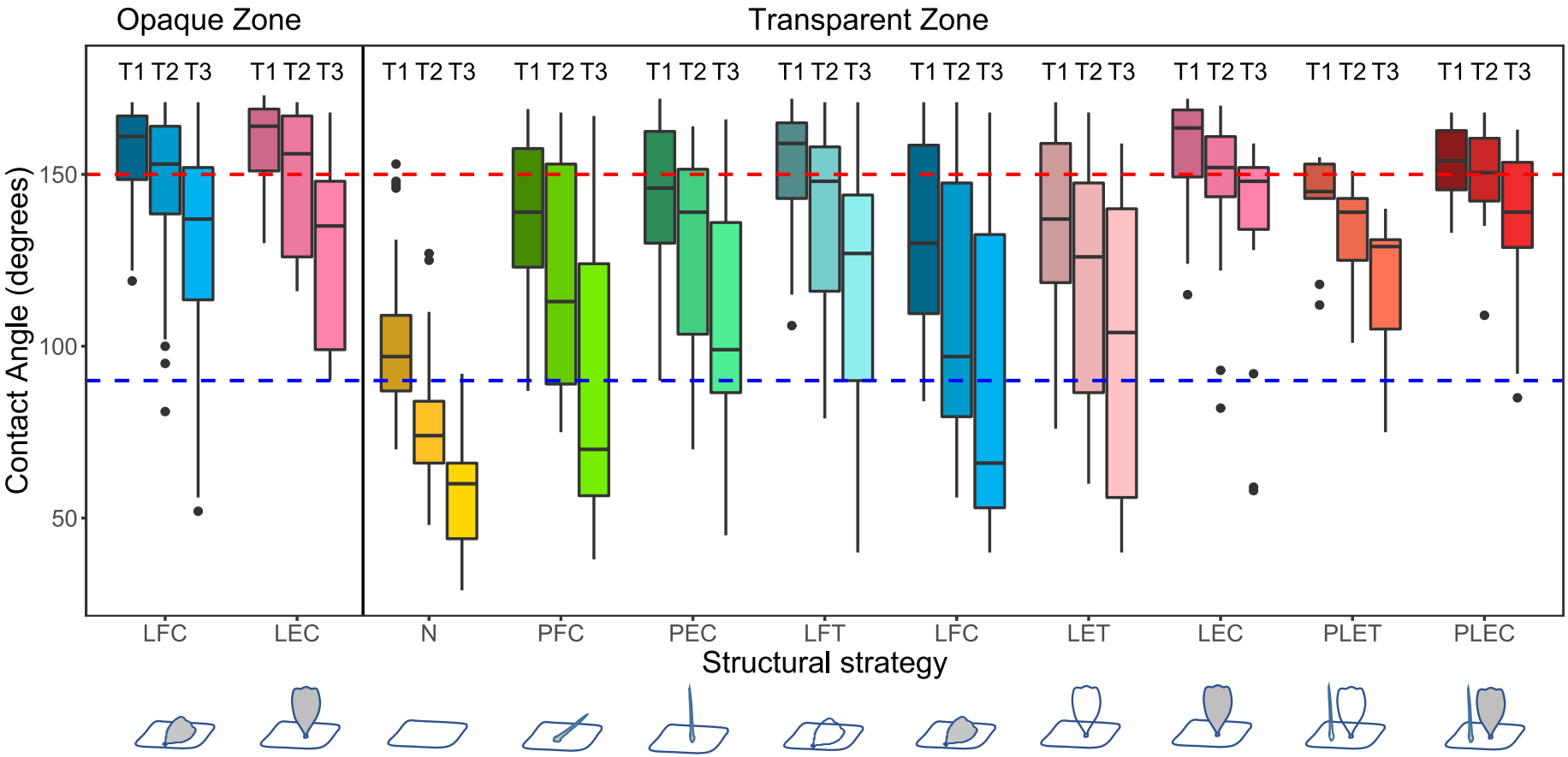

Figure 5. Variations of contact angle with wing zone, microstructure and time, i.e. water droplet size. Structural strategy is a combination of scale type (N: no scales, P: piliform scales, L: lamellar scales, PL: combination of piliform scales and lamellar scales), scale insertion (E: erected, and F: flat), and scale colour (C: coloured, and T: transparent). Superhydrophobic: >150° (above the red line), hydrophobic: <150° and >90°; hydrophilic: <90° (below the blue line). All individuals and droplets were considered. Results are presented in Tables S2 to S3d.

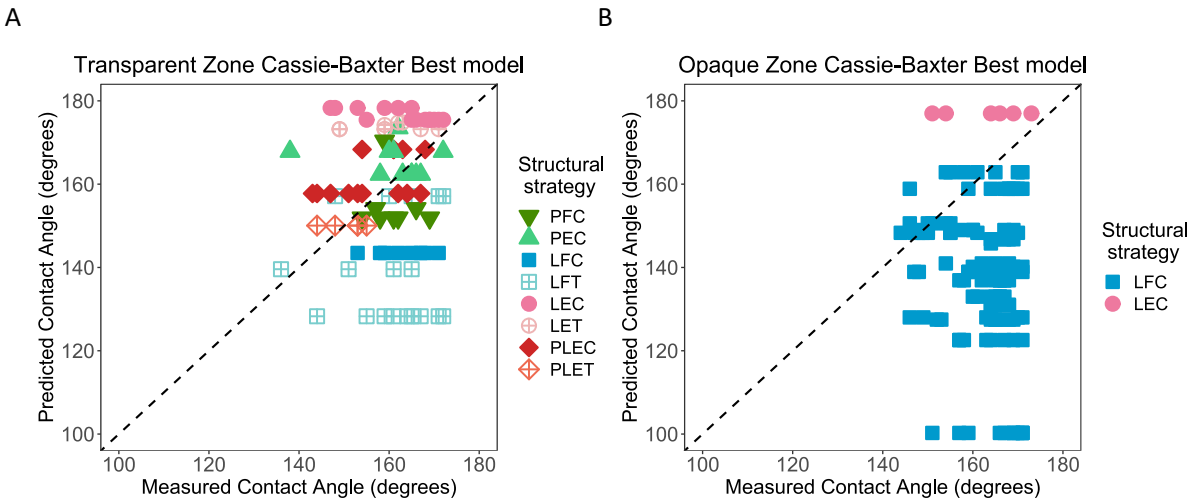

Figure 6. Comparison between contact angle values predicted by the best Cassie-Baxter model for the transparent zone (A) and the opaque zone (B). For the measured values, we included all the values from water droplets characterized as following a Cassie-Baxter regime, i.e. showing a CA>120° at T3. The best model considered the effect of microstructures for all structural strategies (with bending P scales when erect) and an effect of nanostructures, but only for flat lamellar scales in high coverage. Structural strategy is a combination of scale type (N: no scales, P: piliform scales, L: lamellar scales, PL: combination of piliform scales and lamellar scales), scale insertion (E: erect, and F: flat), and scale colour (C: coloured, and T: transparent). The dashed black line represents perfect agreement between prediction and measurement. We considered all the measured water droplets, and for time T1.

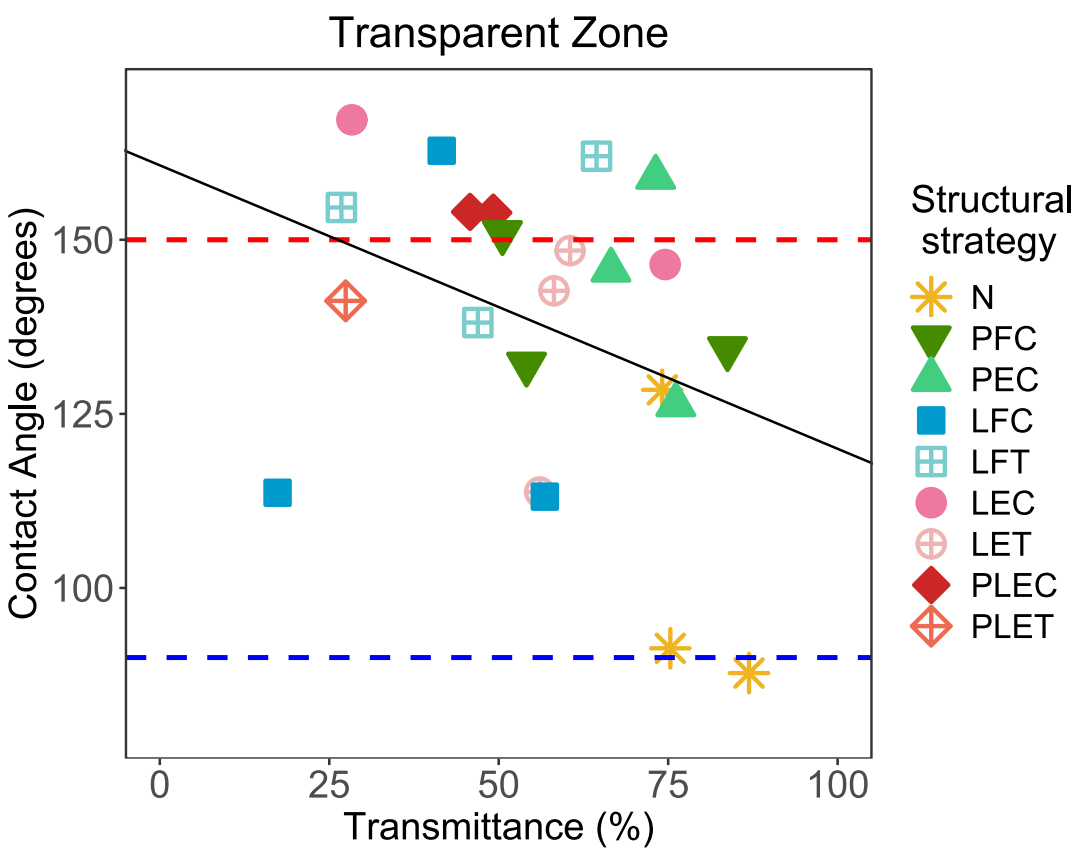

Figure 7. Variations of contact angle with wing transmittance for the different structural strategies. Structural strategy is a combination of scale type (N: no scales, P: piliform scales, L: lamellar scales, PL: combination of piliform scales and lamellar scales), scale insertion (E: erected, and F: flat), and scale colour (C: coloured, and T: transparent). Superhydrophobic: >150° (above the red line), hydrophobic: <150° and >90°; hydrophilic: <90° (below the blue line). We considered only the mean of CA for each species, for time T1, and for the transparent zone. The black plain line indicates the significant fitted regression line based on the Bayesian model. Results are presented in Table S5.

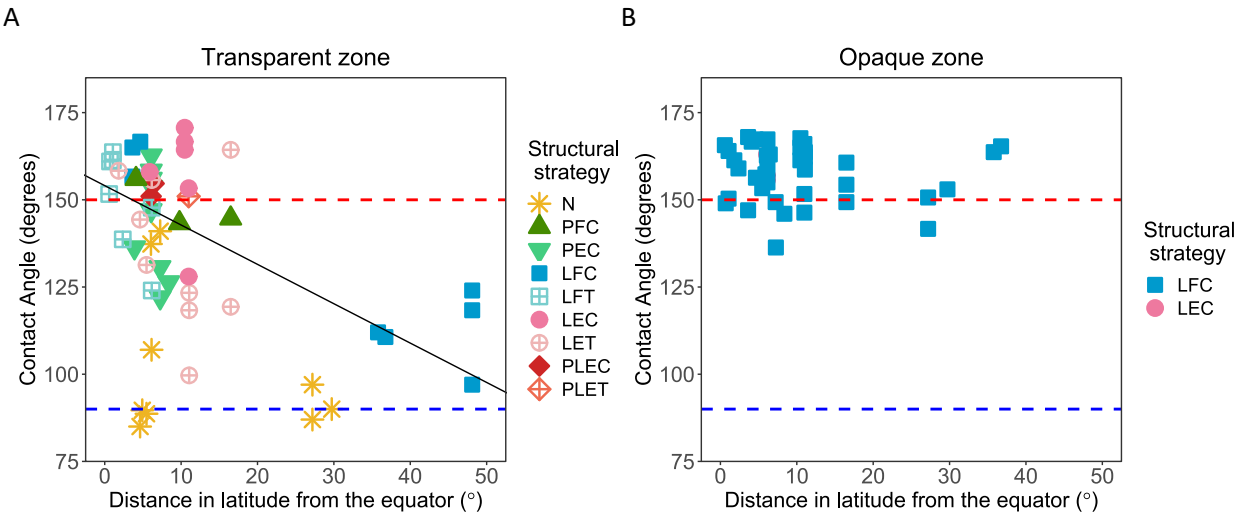

Figure 8. Relationship between contact angle in the transparent (A) and in the opaque (B) zone and the distance in latitude to the equator. Structural strategy is a combination of scale type (N: no scales, P: piliform scales, L: lamellar scales, PL: combination of piliform scales and lamellar scales), scale insertion (E: erected, and F: flat), and scale colour (C: coloured, and T: transparent). Superhydrophobic: >150° (above the red line), hydrophobic: <150° and >90°; hydrophilic: <90° (below the blue line). The black plain line in A indicates the significant fitted regression line based on the Bayesian model. Results are presented in Table S6.